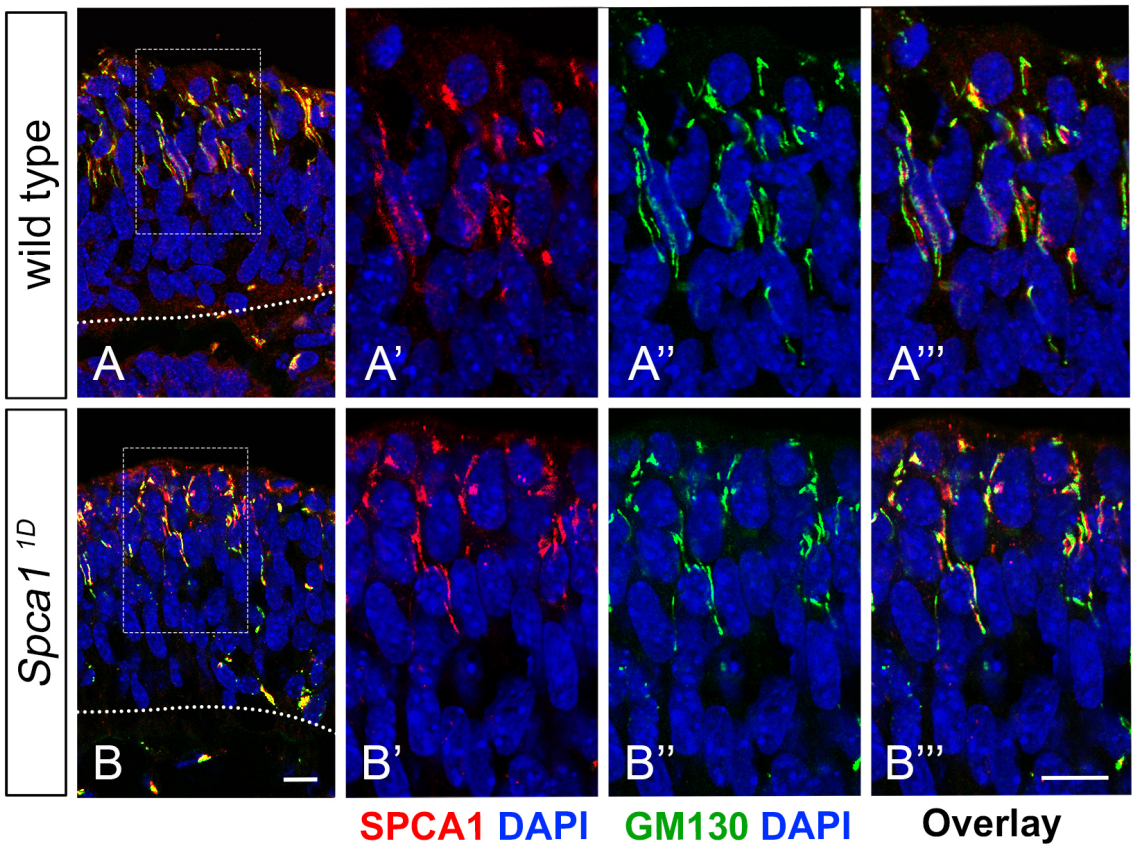

Figure S1. SPCA1^{1D} localization to Golgi in E9.5 neural epithelia. (A-B) Immunodetection of SPCA1 (red) and the cis-Golgi marker GM130 (green) in wild type (A) and *Spca1*^{1D} mutants (B). Cell nuclei are labelled with DAPI staining (blue). Scale bars = 10 μm.

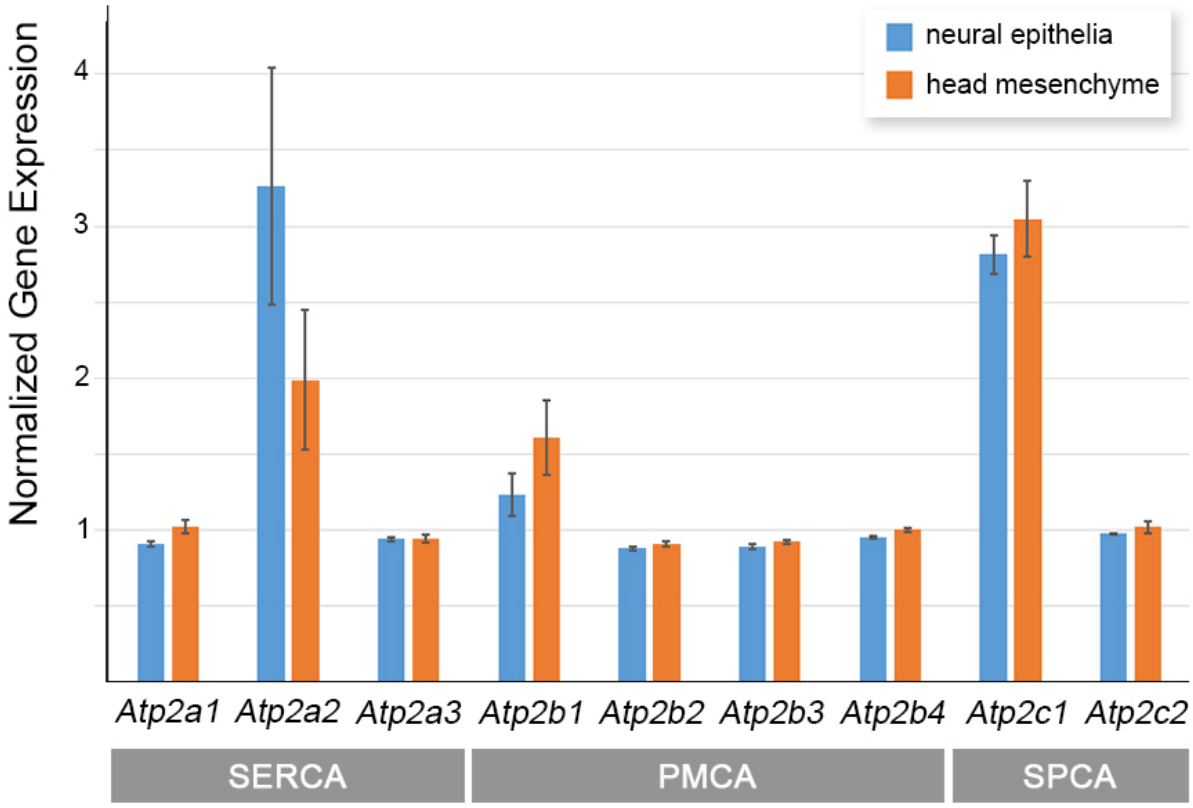

Figure S2. Relative abundance of calcium ATPases in neural epithelia. Graph showing normalized gene expression for calcium ATPases of the SERCA, PMCA and SPCA families in neural epithelia and head mesenchyme tissues dissected by laser-capture and analyzed by RNA-seq in {Brunskill:2014dj}.

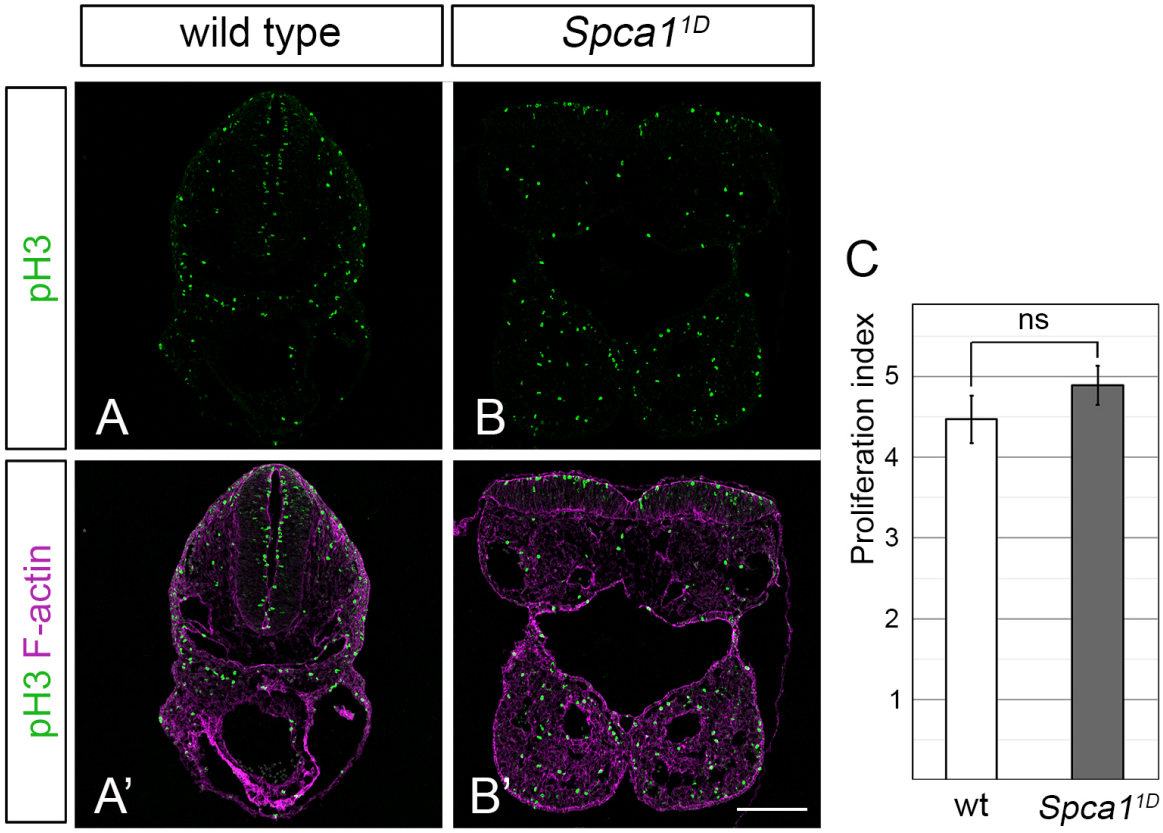

Figure S3. Cell proliferation in *Spca1^{1D}* mutants. (A-B, A'-B') Immunodetection of the proliferative marker phospho-Histone3 (green) and F-actin (magenta) in E9.5 wild type and *Spca1^{1D}* embryonic sections. Scale bar = 200 µm. (C) Plot showing the average proliferative index (pH3 positive foci / total number of nuclei) in E9.5 wild type (n=12 sections from 4 embryos) and *Spca1^{1D}* (n=10 sections from 3 embryos) neuroepithelia (pH3 positive foci / total number of nuclei).

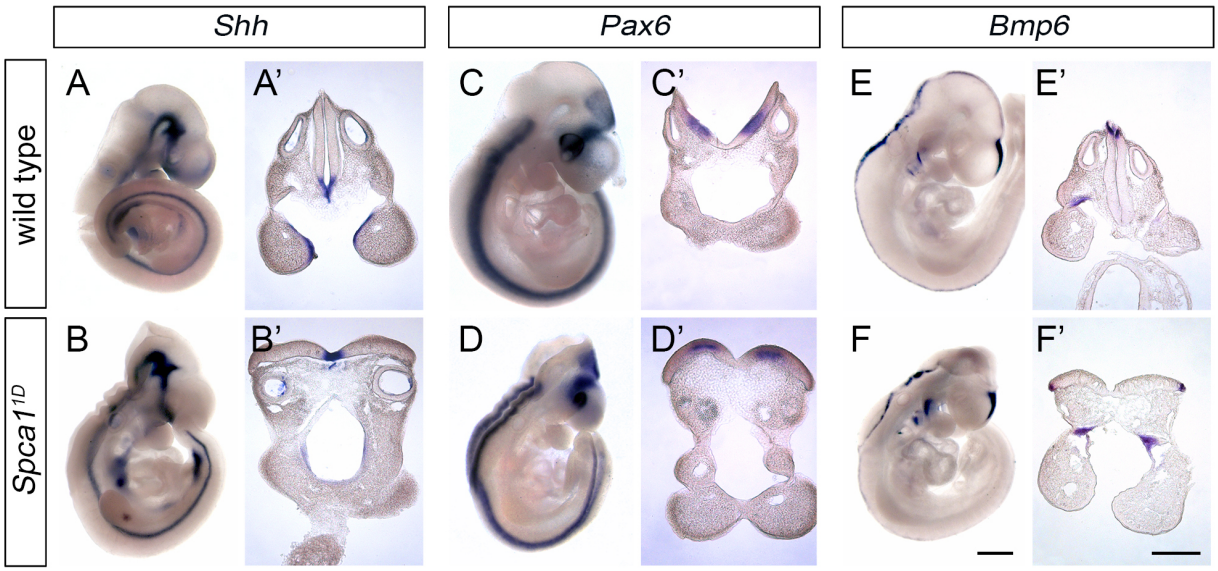

Figure S4. Neural tube dorso-ventral patterning in *Spca1*^{1D} mutants. In situ hybridizations for the notochord and floorplate marker *Shh* (A-B), the ventral neuronal marker *Pax6* (C-D), and the dorsal marker *Bmp6* (E-F) in E9.5 wild type and *Spca1*^{1D} mutants. Transverse sections at the hindbrain region are shown in A'-F'. Scale bars = 500 μm (whole-mount embryos) and 100 μm (sections).

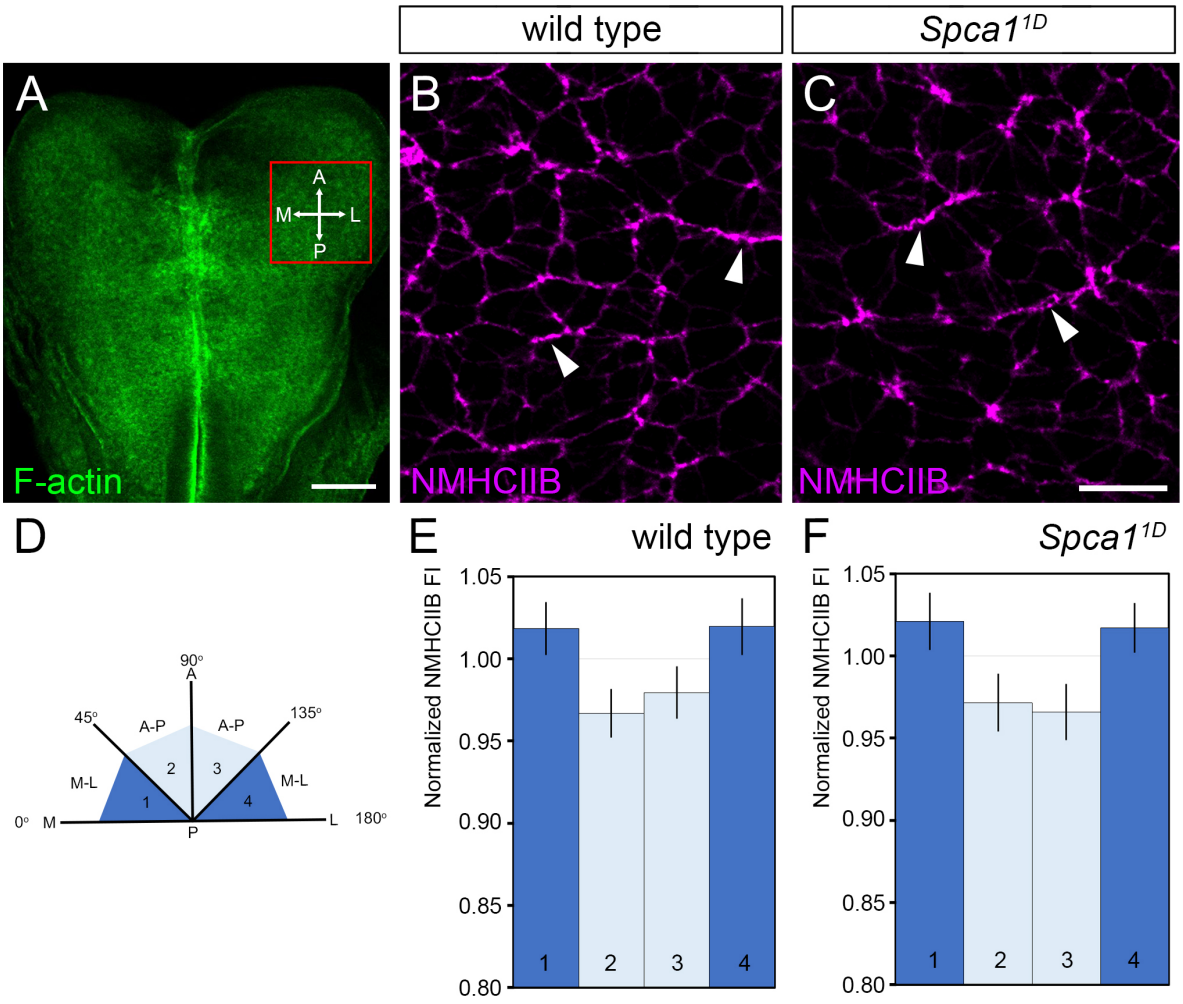

Figure S5. Planar cell polarity in *Spca1^{1D}* mutants. En face view of an E8.5 wild type neuroepithelium stained with phalloidin (A) showing the orientation and position (red box) for images in B and C. Scale bar = 100 μm. A – anterior, P – posterior, L – lateral, M – medial. (B-C) Representative *en face* views of E8.5 wild type and *Spca1^{1D}* neuroepithelia immunostained with NMHCIIB. Both wild type and *Spca1^{1D}* neuroepithelia showed a preferential localization of NMHCIIB at junctions along the M-L axis (white arrowheads). Scale bar = 10 μm. (D) Diagram describing the bins used for quantification. Junctions oriented within 45^{o} of the M-L axis were designated M-L junctions (bins 1 & 4, dark blue). Junctions oriented greater than 45^{o}-90^{o} from the M-L axis were designated A-P junctions (bins 2 & 3, light blue). (E-F) Quantification of NMHCIIB junctional fluorescence intensities. NMHCIIB was similarly enriched along M-L junctions in wild type and *Spca1^{1D}* neuroepithelia, arguing that loss of SPCA1 does not disrupt planar cell polarity in this tissue. Data corresponds to >400 total junctions from 3 different embryos per condition. Representative examples of the samples quantified in E-F are shown in B-C. Error bars indicate SEM.

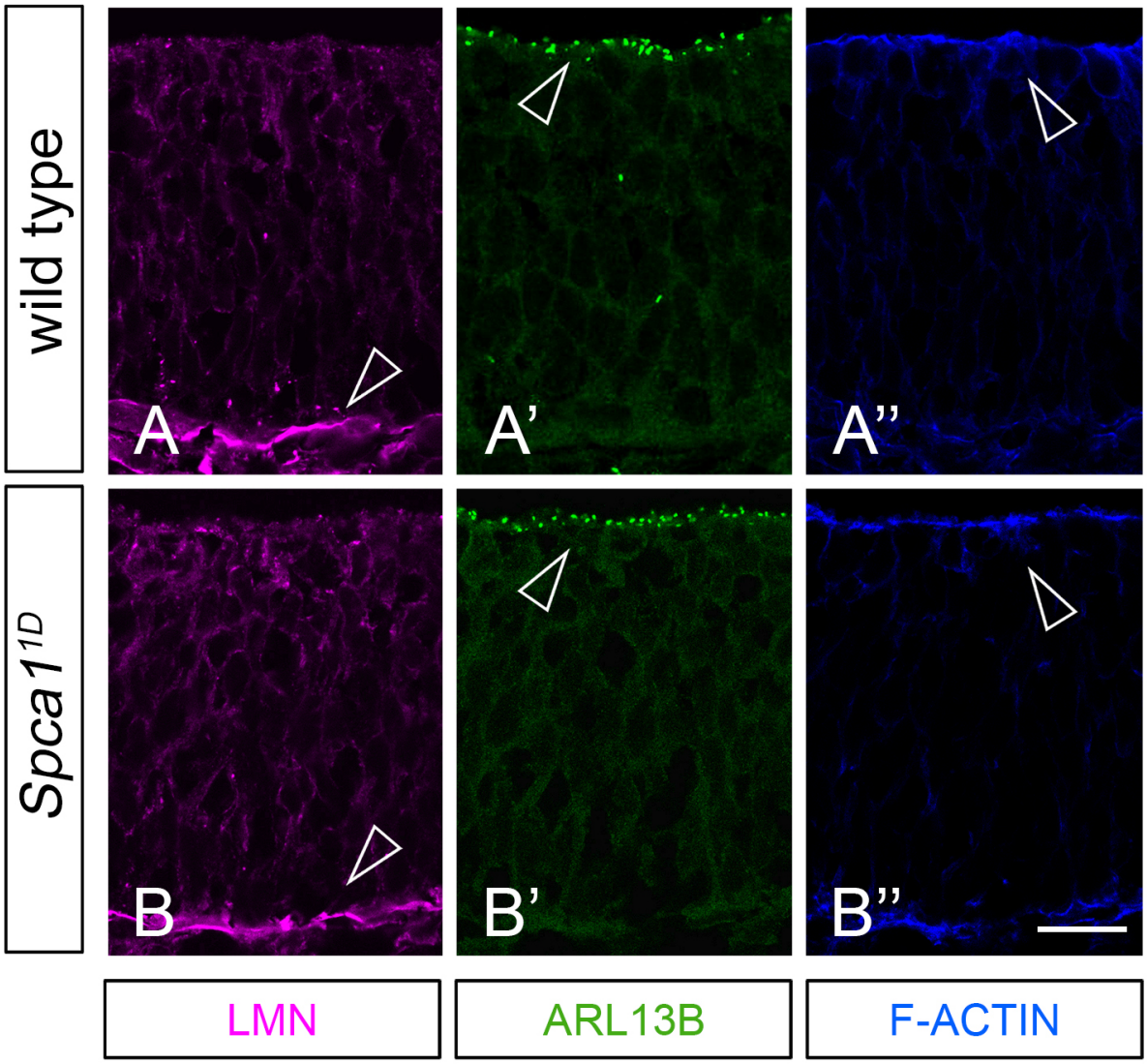

Figure S6. Apico-basal polarity in *Spca1^{1D}* mutants. Immunodetection of markers of apico-basal polarity in E9.5 wild type (A-A"') and *Spca1^{1D}* (B-B"') embryonic sections. Empty arrowheads point to the basal localization of laminin (LMN, magenta), the apical localization of the cilia marker ARL13B (green), and the apical accumulation of F-actin (blue). Scale bar = 20 μm.

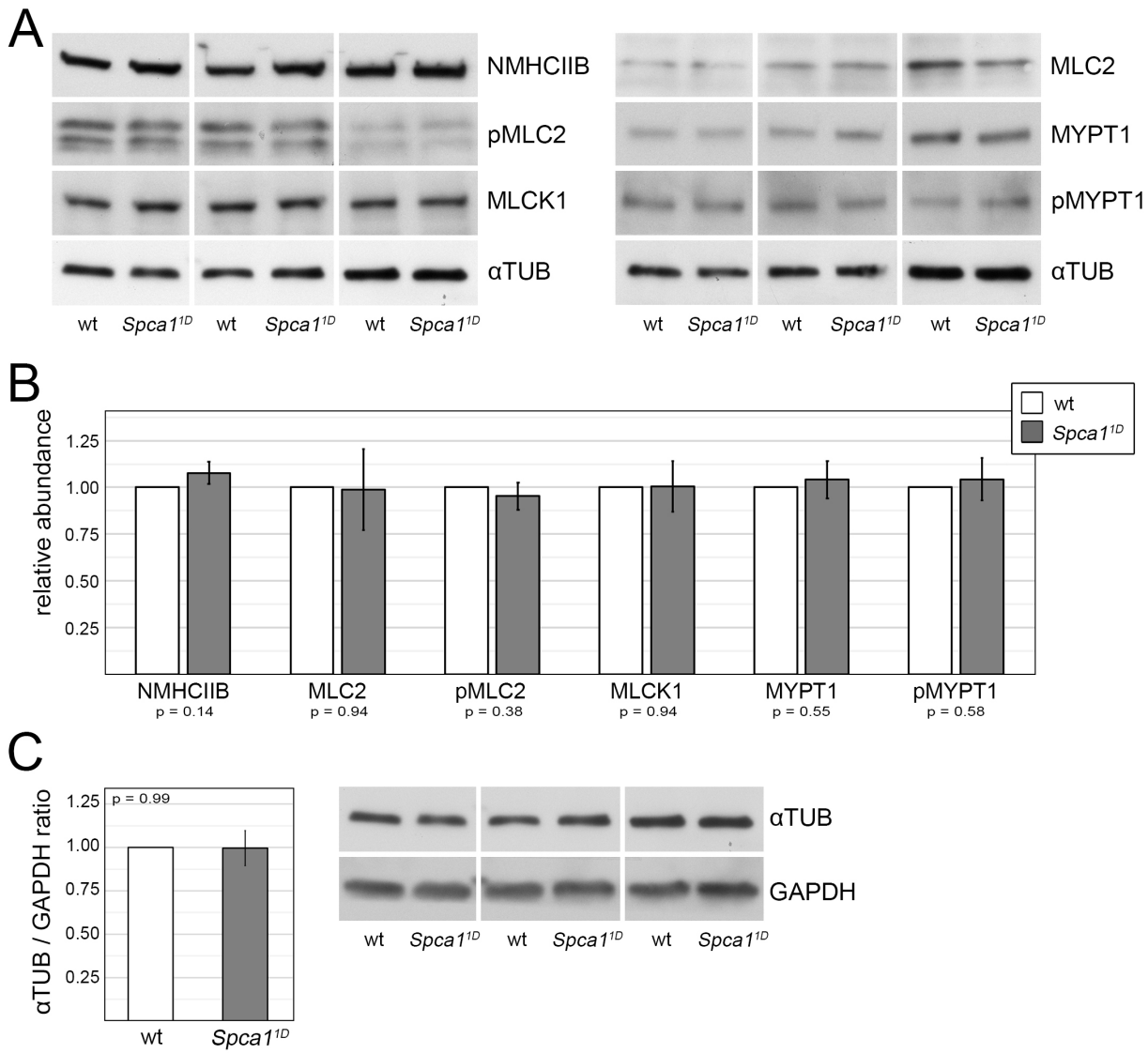

Figure S7. Analysis of myosin regulation in *Spca1^1D* mutants. Western blot experiments were used to quantify the levels of NMHCIIB, MLC2, pMLC2, MLCK1, MYPT1 and pMYPT1 (A) in E9.5 protein extracts from wild type and *Spca1^1D* embryos. Results are shown for 3 biological replicates. (B) Graphs represent the quantification of protein abundance, as normalized to αTubulin and relative to their wild type control. (C) Comparison of αTubulin and GAPDH levels in wild type and *Spca1^1D* embryos, confirming that the use of αTubulin as loading control should not affect the accuracy of protein quantification in *Spca1^1D* mutants. Error bars represent standard deviation. P-values were calculated using Student's paired T-test.

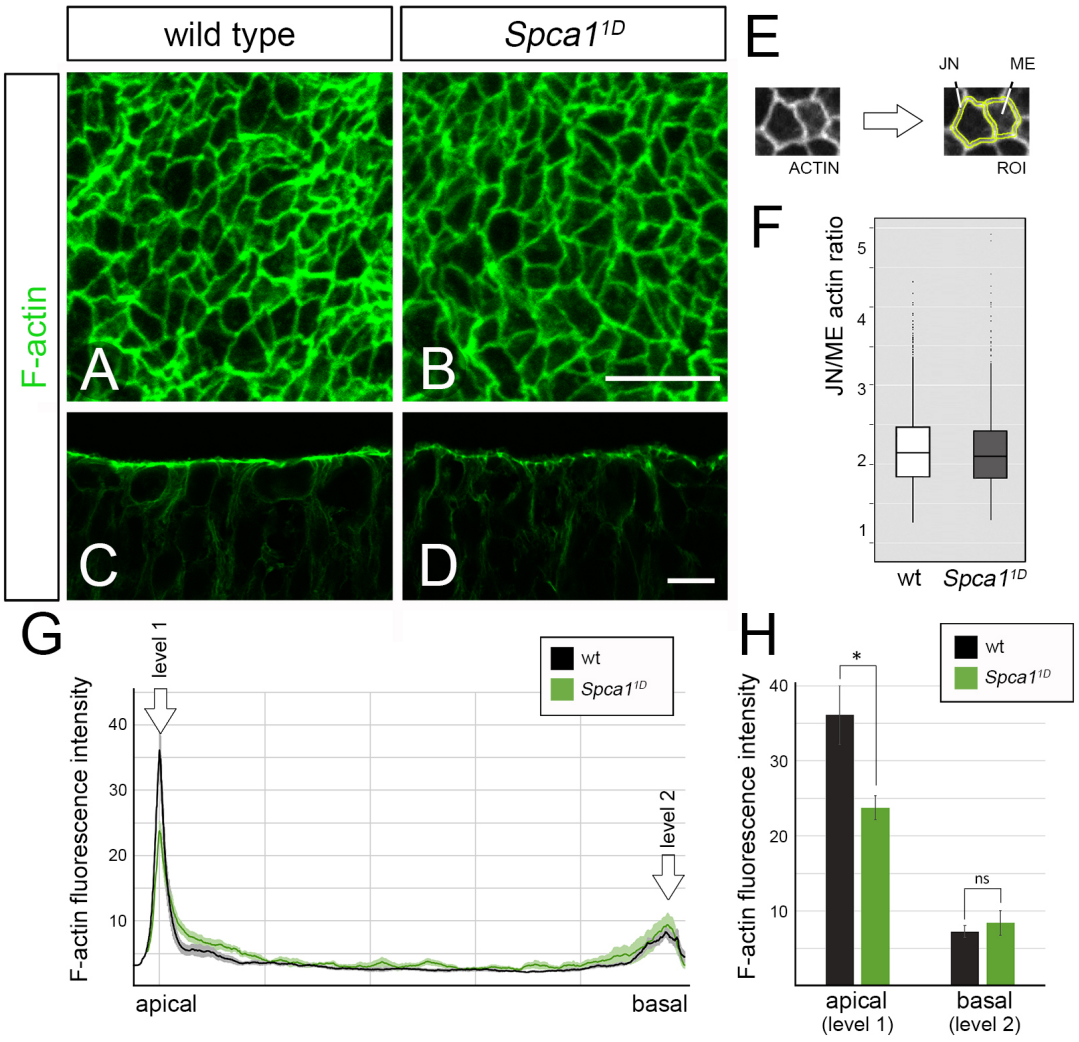

Figure S8. F-actin localization in *Spca1^{1D}* mutants. *En face* views (A-B) and transverse sections (C-D) of E9.5 wild type and *Spca1^{1D}* neuroepithelia stained with phalloidin to reveal F-actin. Scale bars = 10 μm. (E) Methodology for the establishment of regions of interest (ROI) used in the quantification of junctional and medial F-actin (panel F) and NMHCIIB (Figure 6C). (F) Quantification of junctional to medial actin ratios in E9.5 wild type and *Spca1^{1D}* embryos. Data corresponds to >1000 cells from 4 different embryos per condition. Representative examples of the samples quantified in D are shown in A-B. (G-H) Intensity plot showing F-actin accumulation at different levels of the neuroepithelia in E9.5 wild type and *Spca1^{1D}* mutants. Data was quantified from 8 wild type and 6 *Spca1^{1D}* images corresponding to 4 embryos per condition. The X axis indicates the position along the apico-basal axis as a % of the total height of each neuroepithelial sample. Arrows in G indicate F-actin fluorescence intensity at the two levels shown in panel H. Representative examples of the samples quantified in G and H are shown in C-D. P-values ns-not significant, * <0.05

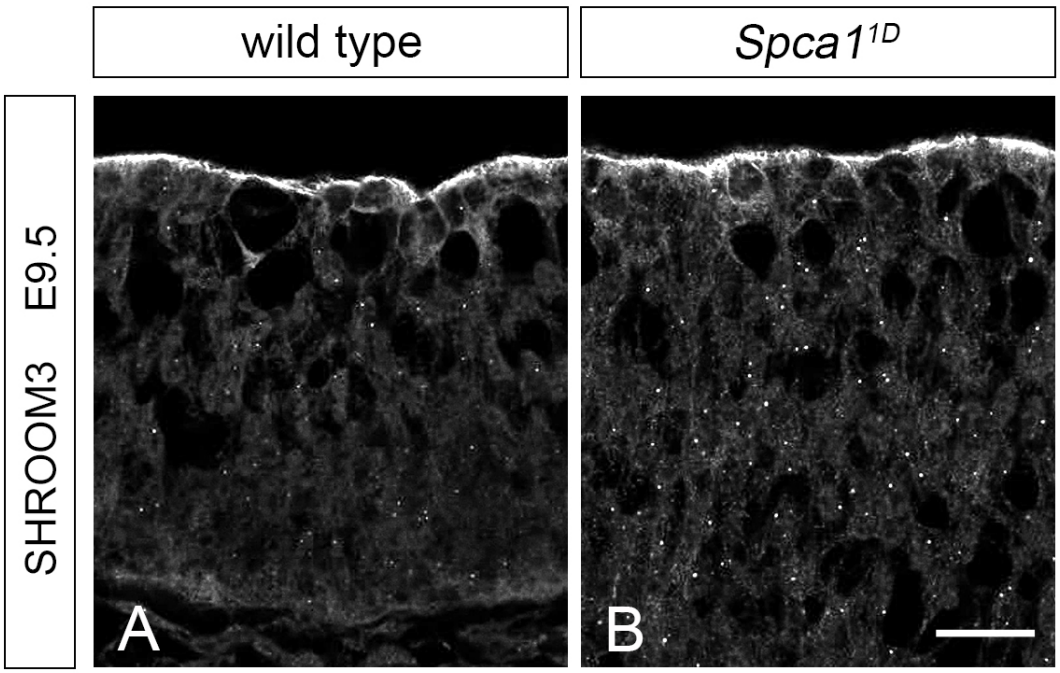

Figure S9. SHROOM3 localization in *Spca1*^{1D} mutants. Immunodetection of SHROOM3 in transverse sections of E9.5 wild type and *Spca1*^{1D} neuroepithelia. Scale bars = 20 μm.

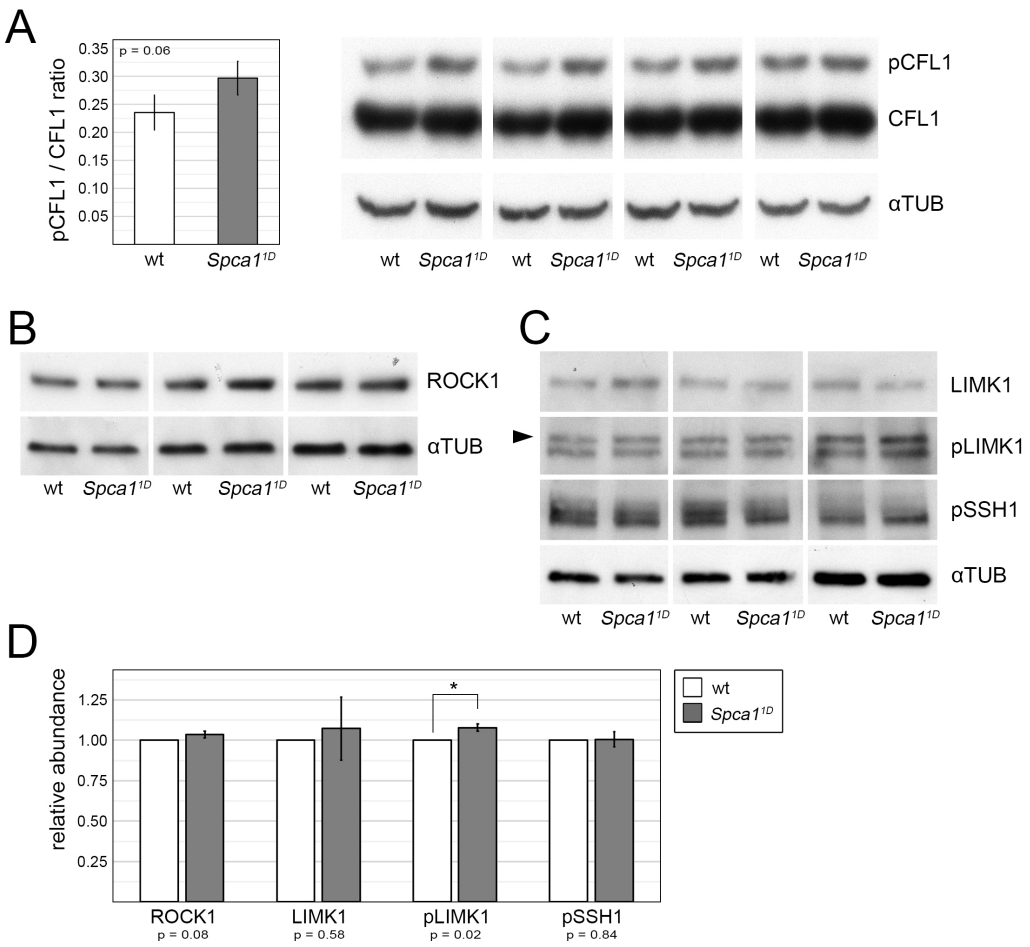

Figure S10. Analysis of CFL1 phosphorylation in *Spca1^{1D}* mutants. Western blot experiments were used to quantify the levels of (A) pCFL1, CFL, (B) ROCK1, (C) LIMK1, pLIMK and pSSH1 in E9.5 protein extracts from wild type and *Spca1^{1D}* embryos. Results are shown for 4 (A) and 3 (B, C) biological replicates. Graphs represent the quantification of pCLF1 to CFL1 ratio (A) and protein abundance as normalized to αTubulin and relative to their wild type control (D). We found that the pCFL1 to CFL1 ratio was elevated by an average of 26% in neural tube extracts from *Spca1^{1D}* mutants, although this difference was not statistically significant (A, p=0.066). The levels of ROCK1, pSSH1 and LIMK1 were not affected in *Spca1^{1D}* embryos (B-D). However, we detected a small, but statistically significant increase in the levels of pLIMK1 in *Spca1^{1D}* mutants as compared to littermate controls (C-D, 7% increase, p=0.02). The interpretation of these experiments is limited by the shortcomings of analyzing protein levels through Western blotting in embryonic extracts. Nonetheless, these results raise the possibility that loss of *Spca1* activity might cause significant local differences in pCFL1 and pLIMK1 levels that, although difficult to detect as significant through Western blotting experiments, could ultimately be responsible for the abnormal CFL1 localization we observed in *Spca1* mutants. Error bars represent standard deviation. P-values were calculated using Student's paired T-test.

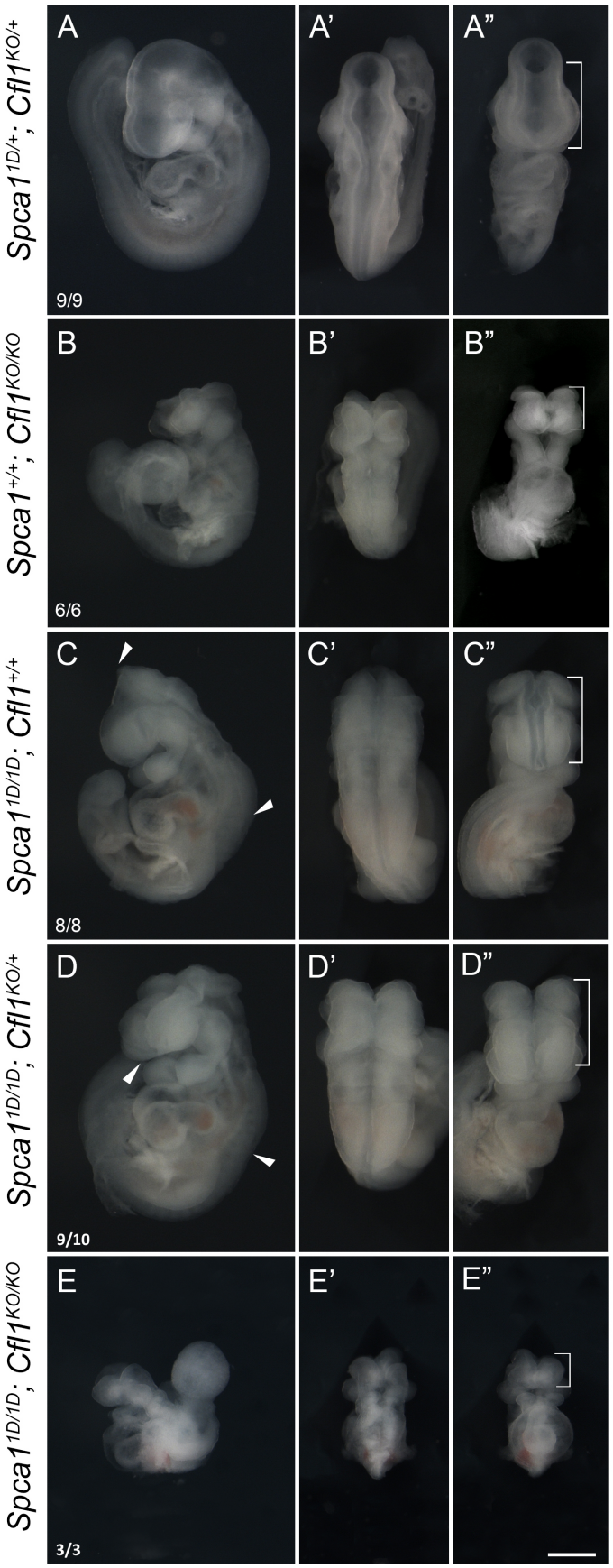

Figure S11. Phenotypic analysis of embryos carrying *Spca1* and *Cfl1* mutant alleles. See figure legend in following page.

Figure S11. Phenotypic analysis of embryos carrying *Spca1* and *Cfl1* mutant alleles. Lateral (A-E), dorsal (A'-E') and frontal (A"-E") views of double heterozygote for *Spca1*$^{1D/+}$; *Cfl1*$^{KO/+}$ embryos (A-A"), homozygote *Cfl1*^{KO} embryos (B-B"), homozygote *Spca1*^{1D} embryos (C-C"), *Spca1*^{1D} mutants lacking one allele of *Cfl1* (*Spca1*^{1D} ; *Cfl1*$^{KO/+}$ embryos, D-D") and double homozygote *Spca1*^{1D} ; *Cfl1*^{KO} embryos (E-E"). We failed to detect any genetic interaction in double heterozygote *Spca1*$^{1D/+}$; *Cfl1*$^{KO/+}$ embryos, which were undistinguishable from wild type controls (A-A"). However, we found that embryos mutant for *Spca1* and lacking one dose of *Cfl1* showed forebrain exencephaly with high penetrance (9/10 embryos). Forebrain exencephaly is characteristic of *Cfl1* mutants (B-B"), but is never observed in heterozygote *Cfl1* embryos and only sporadically seen in homozygote *Spca1* mutants (2/83). Therefore, the appearance of forebrain exencephaly in *Spca1*^{1D} ; *Cfl1*$^{KO/+}$ embryos suggests that SPCA1 and CFL1 cooperate in promoting neural tube closure. Double homozygote *Spca1*^{1D} ; *Cfl1*^{KO} embryos have an early developmental arrest that precedes that of both *Cfl1* and *Spca1* mutants, a result consistent with both mutations having additive effects on embryonic development. Note that the interpretation of these experiments is complicated by the fact that *Cfl1* has known functions in tissues other than the neural tube, including neural crest and mesoderm (Gurniak et al., 2005). Conversely, *Spca1* is ubiquitously expressed and also required in tissues other than the neural tube, as supported by the generalized apoptosis observed in *Spca1* embryos (Okunade et al., 2007 and Figure 4). Consequently, the genetic interactions observed could be due to additive effects of *Spca1* and *Cfl1* loss of function within the neural tube tissue or to additive non-autonomous effects in other tissues known to influence neural tube closure (Chen and Behringer, 1995; Moury and Schoenwolf, 1995). Arrowheads indicate the extent of the exencephalic phenotype. Brackets highlight the forebrain region. Fractions in A-E indicate the number of embryos showing the phenotype shown. Scale bar = 500 μm

Table S1. Reagents, antibodies and primers used.

Reagent	IF	Western blot (blocking)
rabbit anti-Actin (Cytoskeleton, Inc. AAN01)		1:1,000 (NFDM)
mouse anti-ARL13B (NeuroMab 75-287)	1:200	
rabbit anti-Caspase 3 (Cell Signaling 9661)	1:500	
rabbit anti-CFL (Sigma C8736)	1:1,000	1:24,000 (NFDM)
mouse anti-GAPDH (Thermo MA1-46101)		1:4,000 (NFDM)
mouse anti-GM130 (BD Biosciences 610822)	1:400	
rabbit anti-Laminin (Sigma L9393)	1:50	
rabbit anti-NMHCIIB (Covance PRB-445P)	1:400	1:24,000 (NFDM)
rabbit anti-pH3 (Ser10) (Upstate 06-570)	1:250	
rabbit anti-LIMK1 (Cell Signaling 3842)		1:1,000 (NFDM)
rabbit anti-pLIMK1 (Thr508) (ECM Biosciences LP1891)		1:1,000 (BSA)
rabbit anti-MLC2 (Cell Signaling 3672)		1:1000 (BSA)
rabbit anti-pMLC2 (Ser19) (Cell Signaling 3671/Abcam 2480)		1:1,000 (BSA)
rabbit anti-MLCK (Abcam ab76092)		1:2,000 (BSA)
rabbit anti-MYPT1 (Cell Signaling 2634)		1:1,000 (BSA)
rabbit anti-pMYPT1 (Thr696) (Cell Signaling 5163)		1:1,000 (BSA)
rabbit anti-SHROOM3 (gift from Masatoshi Takeichi, Nishimura and Takeichi 2008)	1:400	
rabbit anti-SPCA1 (gift from Tim Reinhardt, USDA ARS, Cross et al 2013)	1:100	
mouse anti-αTUB (Sigma T6199)		1:24,000 (NFDM)
rabbit anti-ROCK1 (Bethyl Laboratories A300-457A)		1:5,000 (NFDM)
rabbit anti-pSSH1 (Ser978) (ECM Biosciences SP3901)		1:1,000 (BSA)
rat anti-ZO1 (Developmental Studies Hybridoma Bank R26.4C)	1:10	
Alexa-Fluor conjugated goat secondary antibodies (ThermoFisher A11034/A11036)	1:200	
AF488/AF568-Phalloidin (ThermoFisher A12379/A12380)	1:50	

Primer name	Primer sequence	Experiment
Atp2c1-1F	TCCTGCTCCTTCTCCTCGG	Sequencing SPCA1 coding region
Atp2c1-1R	GCCTGCCTCAACAATTCTGC	Sequencing SPCA1 coding region
Atp2c1-2F	CTGAGGTCACTGGAGTTGGC	Sequencing SPCA1 coding region
Atp2c1-2R	ATTGTCTCGAAGCTCTCGCC	Sequencing SPCA1 coding region
Atp2c1-3F	GCCTCGAAACTGGAAGGACA	Sequencing SPCA1 coding region
Atp2c1-3R	TGCCAATAACAGCCCTGAACT	Sequencing SPCA1 coding region
D9Mit-310F	AAATCTTTATCATGAAATAGGGATGC	Genotyping Spca1-1D mice (distal marker)
D9Mit-310R	CCCACCCCATGTGTATCAC	Genotyping Spca1-1D mice (distal marker)
D9Mit-182F	GTGAAATTGGTTATGTAAATGTCTGA	Genotyping Spca1-1D mice (proximal marker)
D9Mit-182R	GAGATGACTAGGGTGAACTGGG	Genotyping Spca1-1D mice (proximal marker)
SKO-CSD-lacF	GCTACCATTACCAGTTGGTCTGGTGTC	Genotyping Spca1-KO mice
SKO-CSD-R	GTAGAAGAGGAAGGGAAATGAAGAGC	Genotyping Spca1-KO mice

Table S2. Linkage analysis of mouse lines from our ENU mutagenesis screen
Linkage analysis of mouse lines from our ENU mutagenesis screen was performed using PCR amplification of polymorphic microsatellite markers developed by MIT and available through MGI (www.informatics.jax.org/) and Ensembl databases (ensembl.org/mouse). The specific primers used were selected for the reliable detection of polymorphisms between the C57BL6/J and FvB/NJ strains in 4% agarose gels run for 1.5 hours.

Click here to Download Table S2